VII International Conference on Computational Methods in Marine Engineering
MARINE 2017
M. Visonneau, P. Queutey and D. Le Touzé (Eds)

PARAMETRIC SEARCH AND OPTIMISATION OF FAST DISPLACEMENT HULL FORMS USING RANS SIMULATIONS OF FULL-SCALE FLOW

MARINE 2017

ERIC BRETSCHER*, STUART E. NORRIS[a], ANDREW J. MASON[b], GREGOR J. MACFARLANE[c] AND JAMES P. DENIER[d]

*, [b] Department of Engineering Science,
The University of Auckland,
Auckland 1010, New Zealand
e-mail: e.bretscher@auckland.ac.nz, a.mason@auckland.ac.nz

[a] Department of Mechanical Engineering,
The University of Auckland,
Auckland 1010, New Zealand
e-mail: s.norris@auckland.ac.nz

[c] National Centre for Maritime Engineering & Hydrodynamics,
Australian Maritime College, University of Tasmania
Launceston, Tasmania 7250, Australia
e-mail: gregorm@amc.edu.au

[d] Department of Mathematics,
Macquarie University, NSW 2109, Australia
e-mail: jim.denier@mq.edu.au

Key words: RANS simulation, parametric modelling, shape optimisation.

Abstract. A methodology to derive parametric hull design candidates with a specified displacement and initial stability is introduced. A gradient-free search and optimisation algorithm coupled to a RANS CFD solver is then used to identify efficient pure-displacement hull shapes with minimal hydrodynamic resistance operating in the transition speed region without relying on dynamic lift.

1 INTRODUCTION

Fast pure-displacement monohull shapes have the potential to offer higher average operating speeds at much lower fuel consumption than planing or semi-displacement craft. Such hulls would be valuable in sectors as diverse as coastal fishing and leisure applications.

Historical research into fast displacement hull forms, as compiled and presented by Oossanen [1], identified that residuary resistance in the upper speed range is primarily a function of the length-to-displacement ratio. While a high length-to-displacement ratio appears to be a necessary condition, it is not in itself sufficient to achieve a low resistance. This paper shows that considerable potential exists to design small craft hull shapes, using viscous flow simulations coupled to an optimisation algorithm, which provide more

economical performance than is commonly found today.

2 PARAMETRIC HULL MODEL

2.1 Formulation

We created a fully parametric numerical hull model based on a nested parameterisation scheme in the modelling software *CAESES V4.1.2* [2]. A hull cross-section model was first constructed using quadratic B-spline segments with 7 control points determined by 10 free variables. A broad diversity of hull cross-sections was able to be modelled, as illustrated in Figure 1. The tri-dimensional hull shape was then specified using control curves that defined values for the cross-section variables along the length of the hull. A bounded 41-dimensional master input parameter vector $\vec{p} \in \mathbb{R}^{41}$, $\overrightarrow{p_l} \leq \vec{p} \leq \overrightarrow{p_u}$, allowed manipulating these control curves.

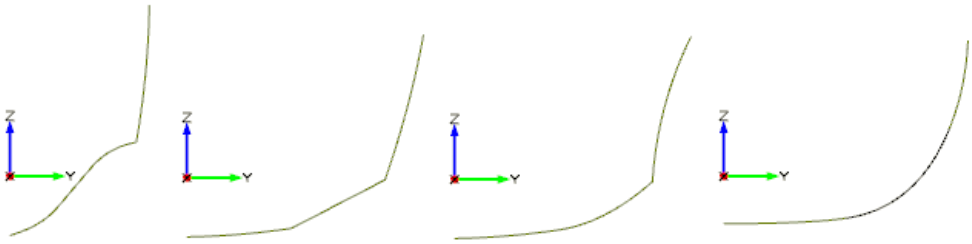

Figure 1: Examples of achievable parametric half-hull cross-sections.

This approach naturally supports the production of fair surfaces through simple continuity and differentiability conditions on the master parameter control curves. Unlike a deformation-based approach, the model is also able to evolve beyond its initial shape, while specific features can still be enforced through the bounds of the input vector as well as the intrinsic definition of the cross-section control curves.

The hull geometries were produced in a Cartesian coordinate system (x, y, z) with its origin at the forward design waterline, where x is positive in the direction of the flow and the static waterplane is set at $z = 0$. The modeller exported hydrostatic data for each hull as well as the geometries, most importantly the longitudinal position of the centre of gravity x_{CG}, which is required for the computation of hull resistance in a free-to-trim situation.

2.2 Design constraint mapping

We eventually aim to solve an optimisation problem to minimise resistance while achieving specified initial stability and displacement targets. We handle these two constraints using a novel strategy to map the designs into an iso-displacement, iso-stable space. This ensures that the optimisation always compares hulls of equal capability, without resorting to normalisation of the hull resistance and the creation of Pareto fronts.

On the basis that, for a given scope of requirements and design intent, the elevation of the centre of gravity is not greatly impacted by the details of the hull shape itself, we specify the initial stability of the hull by setting a target value for the component BM [3], defined as:

$$BM = \frac{I_{WP}}{\nabla} \tag{1}$$

where I_{WP} is the second moment of inertia of the waterplane area S_{WP} with regard to the hull centreline and ∇ is the immersed volume of the hull:

$$I_{WP} = \int_{S_{WP}} y^2 dS = 2 \int_{x=0}^{L_{WL}} \int_{y=0}^{Y(x)} y^2 \, dy \, dx = \frac{2}{3} \int Y(x)^3 \, dx \tag{2}$$

$$\nabla = \int_{V_{Hull,z<0}} dV = \iiint_{V_{Hull,z<0}} dx \, dy \, dz \tag{3}$$

where L_{WL} is the waterline length, and $Y(x)$ is the waterline half-beam at position x. Equations (2) and (3) show that the initial stability and displacement of any hull shape can be altered by scaling its beam by a factor α_y and its depth (measured from the waterline plane $z = 0$) by a factor α_z, giving:

$$I'_{WP}(\alpha_y, \vec{p}) = {\alpha_y}^3 I_{WP}(\vec{p}) \tag{4}$$

$$\nabla'(\alpha_y, \alpha_z, \vec{p}) = \alpha_y \alpha_z \nabla(\vec{p}) \tag{5}$$

The metacentric height *BM'* for the scaled design then becomes:

$$BM'(\alpha_y, \alpha_z, \vec{p}) = \frac{{\alpha_y}^2}{\alpha_z} \frac{I_{WP}(\vec{p})}{\nabla(\vec{p})} = \frac{{\alpha_y}^2}{\alpha_z} BM(\vec{p}) \tag{6}$$

If we assign the design target values $BM' = BM_{Target}$ and $\nabla' = \nabla_{Target}$, equations (5) and (6) form a trivial non-linear system that can be solved analytically for α_y (7) and α_z (8) in order to obtain a design based on parameters $\vec{p}$ satisfying equality constraints on displacement and metacentric height.

$$\alpha_y = \sqrt[3]{\frac{\nabla_{Target} \cdot \mathrm{BM}_{Target}}{I_{WP}}} \tag{7}$$

$$\alpha_z = \frac{1}{\alpha_y} \frac{\nabla_{Target}}{\nabla} \tag{8}$$

This transformation was programmatically automated within the parametric geometry modeller by performing a preliminary hydrostatic calculation followed by a subsequent scale transformation.

Lastly, it must be noted that hull beam and depth as such have no relevance within the set of design parameters and must be excluded, as they are uniquely determined by the final transformation.

3 RANS COMPUTATIONAL MODEL

The resistance of each candidate hull was calculated with *Star-CCM+ V11.04.010R8,* a code frequently used for hydrodynamic performance predictions of both displacement [4] and planing craft [5]. The problem was configured using the volume of fluid (*VoF*) formulation and high-resolution interface capture (*HRIC*) scheme to model the free surface. All simulations were conducted for calm water resistance in a free-to-heave and free-to-trim

attitude. The *HRIC* scheme was configured to minimise numerical ventilation issues by preventing a switch to upwind differencing regardless of the local Courant number [6].

The computations employed a transient implicit formulation using the *SIMPLE* algorithm with a maximum of 8 iterations per time step. The flow was modelled as fully turbulent using the two-equation $k-\omega$ shear-stress transport model with an inlet turbulence intensity of 1%. Particular attention was placed on converging the solution down to very small residual errors.

3.1 Modelling motion

Hull motion was handled through the use of an overset mesh block encompassing the hull geometry. Care was taken to preserve compatible cell refinement sizes between the overset and background meshes, in accordance with the *Star-CCM+* guidelines [7]. The width of the overset block was, following a sensitivity study, chosen as $0.3 \cdot L_{WL}$ in order to ensure that disturbances were not introduced into the formation of the divergent wave system; its length was minimised as much as possible to reduce rotation-induced mesh shear effects forward and astern of the hull.

3.2 Computational domain

The computations were carried out in a fluid domain simulating deep, open water for half a hull using a symmetry plane at $y = 0$. The origin of the computational domain was coincident with the origin point of the hull geometries at rest. The dimensions of the fluid domain are documented in Table 1.

Table 1: Relative dimensions of the computational domain

Length	8.0	L/L_{WL}
Width	2.4	W/L_{WL}
Water depth	1.8	H/L_{WL}
Inlet boundary distance	-1.3	$x_{\mathrm{Inlet}}/L_{WL}$

The length of the domain was established keeping in mind that the length of the transverse wave system increases with the square of the velocity and the insensitivity of the solution to the position of these boundaries was verified by performing systematic variations in distance between the stern and the outlet boundary.

3.3 Boundary conditions

The conditions applied at the domain boundaries varied between open water simulations and the simulation of tank experiments for validation (Table 2).

Inlet boundaries made use of the flat wave model available in Star-CCM+. The inlet flow velocity was ramped using a sine function from zero to the target simulation speed in 3 seconds and a momentum source based on the derivative of the inlet velocity profile was introduced into the fluid domain to deliver a matching acceleration. This approach produced stable solutions more quickly than an impulsive start, particularly in the upper speed range.

Table 2: Boundary type assignments

Boundary	Type
Inlet	Velocity inlet
Outlet	Pressure outlet
Symmetry plane	Symmetry
Side	Free-slip wall
Bottom	Free-slip wall
Atmosphere	Velocity inlet

3.4 Mesh

A flow-aligned, trimmed, hexahedral mesh with local anisotropic refinement was used. The free-surface region was vertically refined uniformly throughout the domain and the wake region was further refined in the horizontal plane using block definitions aligned with the Kelvin wake angle [8]. Departing from common practices for ship hydrodynamics, significant additional refinement of the deep water body directly underneath and aft of the hull was introduced (Figure 2) in order to improve the behaviour of the solutions for simulations at Froude numbers $Fr \geq 0.6$.

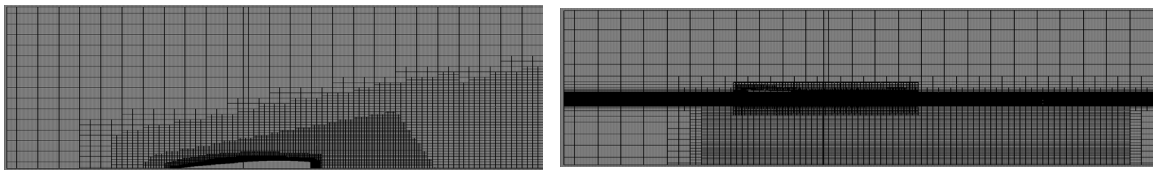

Figure 2: Mesh refinement regions.

A combination of numerical wave damping and planar mesh coarsening was utilised to minimise reflections both at the inlet and outlet boundaries of the domain. The primary concern was avoiding reflection of the long transverse wavelengths produced in the upper speed range and modelling the wake accurately (Figure 3).

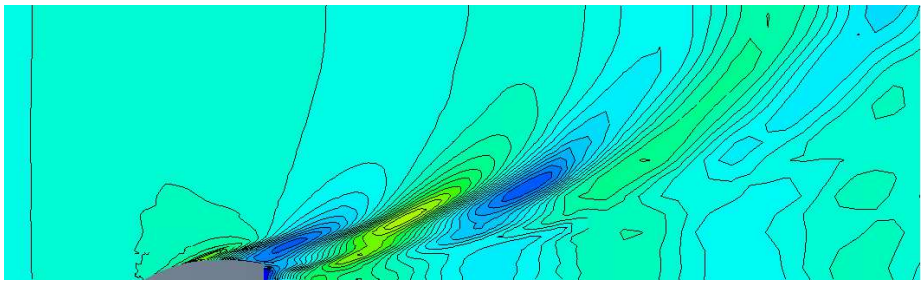

Figure 3: Half-wake for a fast displacement hull candidate at $Fr = 0.6$ in simulated open water.

The near-wall region was meshed using 8 inflation layers covering 60% of the estimated thickness of the boundary layer at the stern [9]. No meaningful changes in viscous or pressure forces were found when meshing the full thickness. The first cell height adopted was $y_0 = 0.54 \cdot 10^{-3} \cdot L_{WL}$, following a convergence analysis of the viscous forces, and yielded an

average non-dimensional value of $y^+ \cong 45$ at a Froude number $Fr = 0.6$, well into the logarithmic region. A geometric growth rate of 1.25 ensured a uniform size transition into the core mesh.

4 EXPERIMENTAL VALIDATION OF COMPUTATIONAL MODEL

4.1 Validation results against DSYHS hulls

We first validated our numerical flow model against the experimental results from selected models within the *Delft Systematic Yacht Hull Series (DSYHS)* [10]. The average magnitude of the error in the predicted resistance over the range $Fr = [0.3\,;\,0.6]$ was 0.9% for hull *SYSSER62*, 1.6% for hull *SYSSER35* and 1.8% for hull *SYSSER48* (Figure 4).

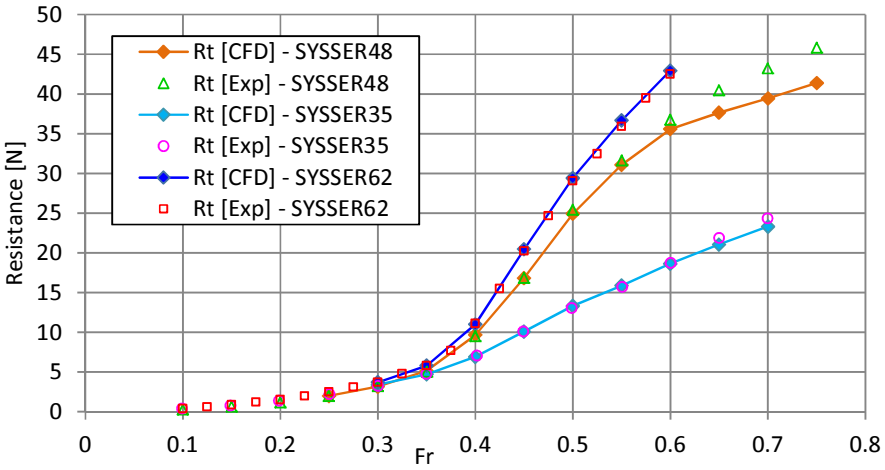

Figure 4: Plot of the experimental and calculated total resistance for selected *Delft* hulls.

We observed deficits in predicted resistance above $Fr = 0.6$ for those hulls for which experimental data was available for such speeds. The bow of the *Delft* yacht hulls lifts out of the water as the dynamic trim increases with speed, leading to a strong pressure point with very high gradients where the blunt hull bottom parts the water. This unwanted phenomenon, which lies beyond the useful speed range of these designs, was imperfectly resolved by our mesh. Since it had no relevance for the type of hulls we were interested in, no further emphasis was placed on modelling it more accurately.

4.2 Validation results against test results at the AMC towing tank

We further tank-tested one of our design candidates, hull *AMC 16-12*, at the *Australian Maritime College Towing Tank* in Launceston, Australia, in compliance with the *ITTC* recommended procedure for calm water resistance tests [10].

Our hull *AMC 16-12* was obtained using the optimisation process described in Section 6 and then built as a towing tank model. Unlike the *Delft* hulls, this design was suitable for operation in the transition speed region, where $Fr = [0.5, 1.0]$ approximately and a wave trough is present in the stern region. The characteristics of the model are detailed in Table 3.

Figure 5: Hull *AMC 16-12* in the towing tank at $Fr = 0.6$.

Table 3: Characteristics of optimised hull model *AMC 16-12*.

Parameter	**Value**	**Unit**
Overall length	1.717	m
Overall beam	0.576	m
Waterline length	1.667	m
Waterline beam	0.399	m
Draft	0.061	m
Displacement	14.133	kg
Wetted surface	0.5117	m^2
BM	0.3	m
x_{CG}	53.2	$\%L_{WL}$
x_{CF}	60.6	$\%L_{WL}$
$L_{WL}/\sqrt[3]{\Delta}$	6.87	-

Comparison between the numerical results and the experimental tests, summarised in Figure 6, Figure 7 and Figure 8, showed that the calculations over-predicted resistance at low speeds by up to 4.8% at $Fr = 0.25$. This discrepancy can be attributed to the fact that the computational mesh was not intended to be capable of resolving the very small and short waves experienced at low speeds, and to the fact that the very low magnitude of the forces being measured may have led to greater experimental uncertainty. In the range $Fr = [0.45, 0.85]$, resistance is consistently under-predicted by an average of -7.44% (Figure 6). We note that this linear error is observable at speeds where all the predictions for the Delft hulls were excellent.

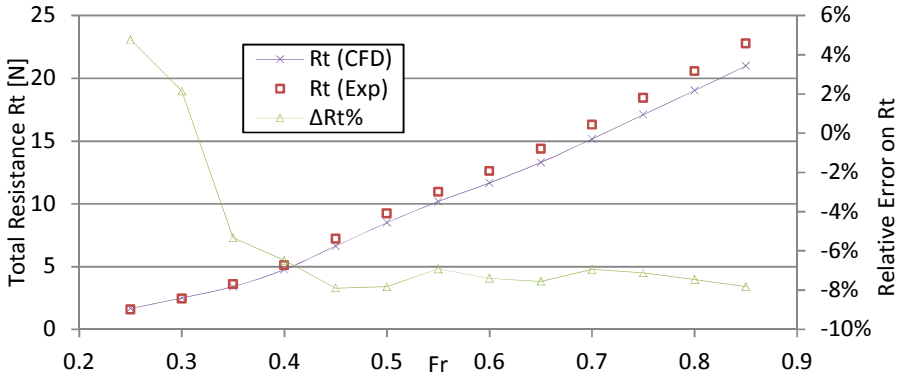

Figure 6: Plots of the experimental and calculated total resistance versus Froude number for hull *AMC-16-12*.

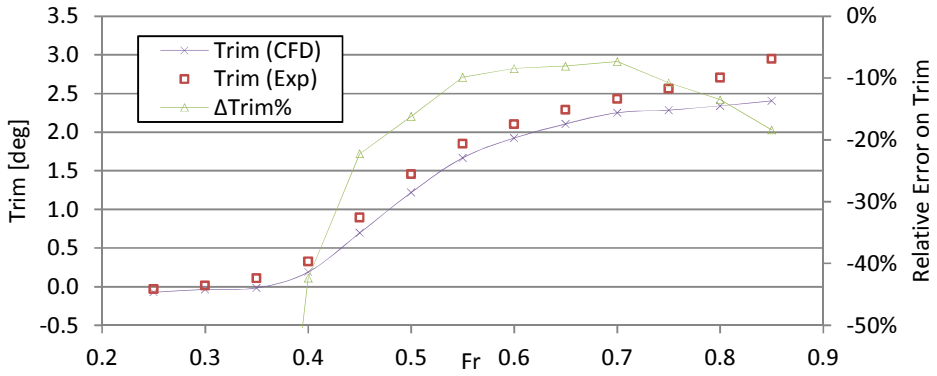

Figure 7: Plots of the experimental and calculated trim versus Froude number for hull *AMC-16-12*.

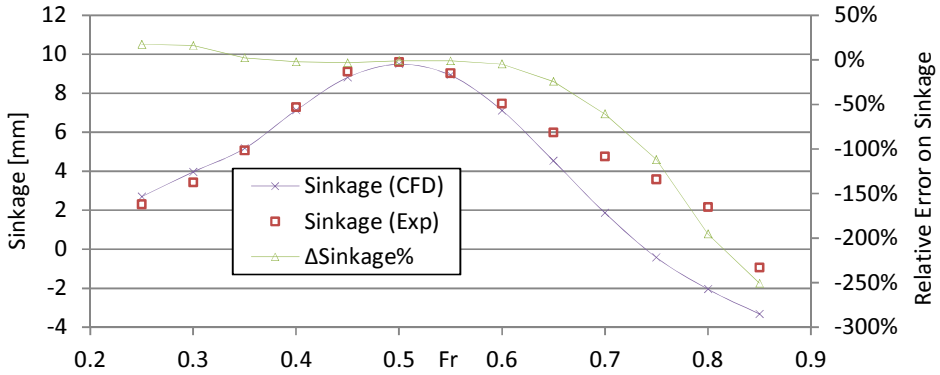

Figure 8: Plots of the experimental and calculated sinkage versus Froude number for hull *AMC-16-12*.

The validity of the simulation was also assessed by comparing the computed dynamic trim (Figure 7) and sinkage (Figure 8) with the experimental data. Trim is consistently under-predicted by a small amount, a result also observed for all *Delft* hulls, but its behaviour is consistent. Sinkage predictions are excellent up to $Fr = 0.6$ and then diverge. Inspection of the time series collected from the tank tests shows that sinkage never reached a steady state

and was still decreasing by the time the higher Froude number runs ended; amongst other known instabilities, the initial acceleration of the towing carriage can result in the model creating a low amplitude wave, which then interferes with the local water level and would require a longer run duration to subside.

5 SOLUTION ACCURACY

An estimate of the solution accuracy was derived from the mesh and time-step convergence studies at the design speed $Fr = 0.6$ used throughout all optimisation runs.

The *Star-CCM+* automated mesher uses a base size specification h_{Base} and locally-defined refinement and coarsening specifications. This size can be normalised against the hull waterline length as $h^* = h_{Base}/L_{WL}$.

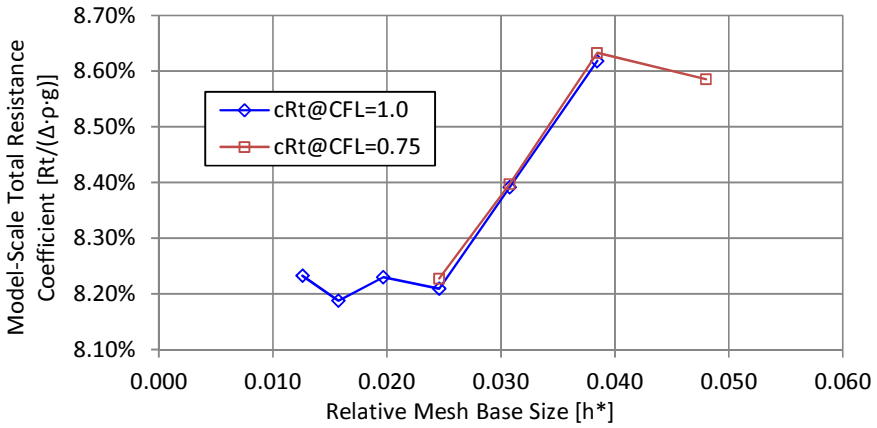

Figure 9: Plot of the convergence of the total resistance coefficient versus mesh size.

The time-step can be expressed non-dimensionally in terms of the Courant number CFL calculated against this base size, which was kept constant throughout mesh size changes. A convergent behaviour was found for $CFL \leq 1.0$. The coarsest mesh needed to be run at $CFL = 0.75$ in order to remain within allowable mesh motion limits at the overset boundary.

Figure 9 presents a plot of the total resistance coefficient versus mesh size, from which we can see a stabilisation for $h^* \leq 0.025\ L_{WL}$ the residual range on the total resistance coefficient is 0.045%. We determined that changes exceeding 0.05% could be considered as meaningful and simulations were conservatively carried out with a mesh base size $h^* = 1.97\%$ at $CFL = 1.0$ in order to avoid numerical ventilation issues for some hull variants.

6 FULL-SCALE RESISTANCE PREDICTION

Due to the differences in the development of the boundary layer, full-scale flow predictions for hull *AMC 16-12* were sufficiently different (Figure 10) from the model-scale results to warrant carrying out hull shape optimisation work either directly at full scale or using an equivalent formulation, rather than relying on an extrapolation method.

We employed the procedure described by *Haase et al.* [11] to seek computed full-scale resistance from the flow simulation work carried out at model-scale by artificially increasing the Reynolds number to its full-scale value by reducing the water kinematic viscosity value.

This solution of the full-scale flow problem at model-scale proved more robust numerically and faster to solve than the true full-scale flow problem. Additional robustness was found without impacting the results by adopting the $k-\varepsilon$ *realisable* turbulence model and a high-y^+ wall function formulation for these simulations.

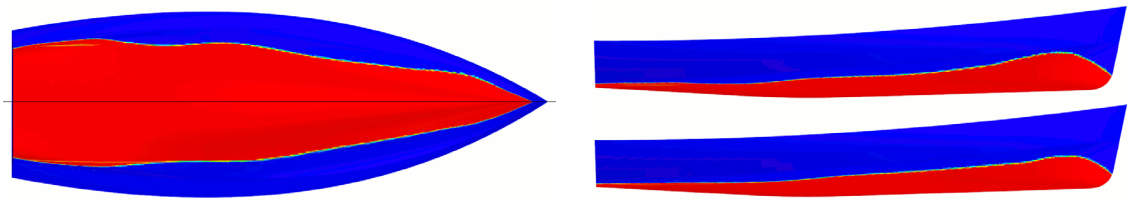

Figure 10: Comparison of the full-scale (top) and model-scale (bottom) computed waterline for hull *AMC 16-12* at $Fr = 0.6$.

While validation of the full-scale resistance prediction is impossible in the absence of experimental data, we compared true full-scale resistance computations to the model-scale values obtained at the same Reynolds number to verify that the result followed the cube of the scale factor as expected. This result was confirmed by *Haase et al.* for slender catamaran hull shapes and it remains applicable for our non-slender hull shapes.

7 DESIGN SEARCH AND OPTIMISATION

7.1 Algorithm

A variety of optimisation algorithms and strategies were considered for this problem. Due to the relatively long CFD computation times required to obtain each hull resistance result, around 1 hour using 32 *Intel x64* cores, we sought an optimisation algorithm both effective in terms of total number of evaluations required and able to exploit parallelism. This weighed against genetic algorithms (parallel with good exploration capabilities, but marginally efficient) and sequential methods such as *Nelder-Mead*. Gradient-based methods, including advanced algorithms using underlying local surrogate models like *sequential quadratic programming*, proved computationally intensive and failed to converge. One common critical issue was a lack of tolerance to failed design evaluations.

We used *Asynchronous Parallel Pattern Search (APPS)* [12], which is a parallel, gradient-free method with reasonable domain exploration capabilities that was specifically intended for such expensive "black box" problems presenting high-dimensionality and a superposition of modelling errors and numerical noise. *APPS* implementations can be found within the packages *Dakota* [13] and *Hopspack* [14]; we retained the *Dakota* implementation as it offers a unified framework for accessing a broad range of evaluation and optimisation tools.

APPS operates by exploring neighbours in a coordinate-search pattern around the current best computed point. For a problem featuring m degrees of freedom, each pattern specifies $2m$ problems to be solved. We ran the *APPS* algorithm as a *Parallel Pattern Search (PPS)* by enabling *blocking synchronisation* and waiting until each pattern had been fully evaluated before formulating new input vectors. This makes a less intensive use of parallelism, but the execution is deterministic and easier to track, interrupt and resume if required.

7.2 Process outline

Our optimisation process was implemented using the solution pipeline shown in Figure 11. The generic optimiser *Dakota* was coupled to the parametric 3D modeller *CAESES* and run on a desktop computer, where it generated the parameter sets for *CAESES*. The resulting 3D geometries and hydrostatic data for the hull design candidates were then uploaded to a HPC cluster to obtain the flow solution at the target design speed from the CFD code *Star-CCM+*. The predicted hull resistance values were then returned to *Dakota*.

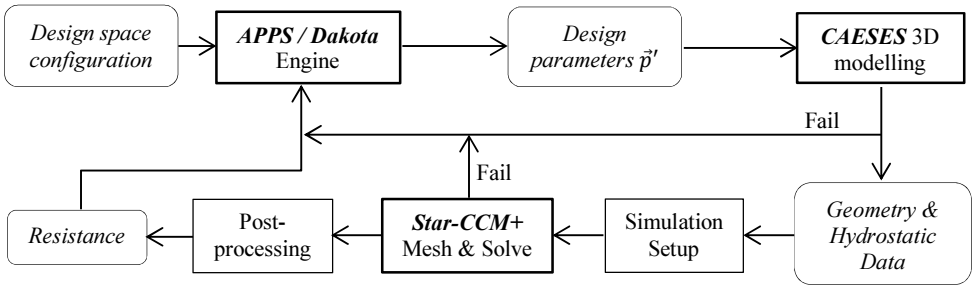

Figure 11: Search and optimisation loop.

It is important to note that failures can occur at times for some designs. These can result from issues in modelling, geometry pre-processing, meshing or solving the flow problem and the optimiser must be able to recover and continue.

7.3 Targets and constraints

As the displacement and stability targets were met using the methodology presented in Section 2.2, only simple bounds were imposed on the design parameters to ensure that the natural validity limits of the geometric model were not exceeded. Some of these limits were also set in order to mandate specific design features and constrain the search within a desired envelope.

Table 4: Design target values at full scale and model scale

Parameter	Full scale	Model scale	Unit
Overall length	20.0	1.717	m
Displacement	22300	14.133	kg
BM	3.49	0.300	m

The target values for the hull displacement and initial stability were obtained from a fast 20-metre aluminium hard-chine lobster fishing boat (Figure 12) originating from Western Australia and surveyed in 2010. These are presented in Table 4 and reflect typical fast modern workboats of moderate displacement and low hull deadrise, where considerable initial stability, limited rolling motion and a lot of aft deck space are sought.

Figure 12: Reference vessel for length, displacement and initial stability targets.

7.4 Initial hull shape and parameters

The initial hull shape was manually designed, drawing on hydrodynamic principles, with the objective of minimising any dynamic lift and run at low trim angles, thus relying primarily on hydrostatic pressure forces to support the hull at speed. The parametric model was then configured to closely approximate this shape and the corresponding parameter vector $\overrightarrow{p_0} \in \mathbb{R}^{41}$ was extracted.

This initial vector was first used in a centred parameter study with a total of 5 sampling points in each dimension. The dimensionality of the problem was then reduced by discarding variables that influenced the hull resistance coefficient by less than 1%. The resulting set was further compressed to 18 parameters by retaining those that showed a potential for improvement greater or equal to 0.2%, leading to an optimisation input vector $\vec{p}' \in \mathbb{R}^{18}$. Reducing the parameter space is by no means a necessity as long as sufficient time or parallel computing capacity is available.

7.5 Hull shape optimisation

Figure 13 shows the solution history from two cascaded optimisation runs, where the second run was started using the best hull design found in the first run. We typically computed up to 36 solutions concurrently approximately every hour, using up to 1152 CPU cores. A total of 652 design variants were produced and 23 successively improved models were found by the algorithm. Thirty-six designs, or 5.5%, were not evaluated due to failures along the modelling and solution pipeline. The search yielded a 15.6% reduction in total resistance over the original hull while preserving the stability component BM and displacement for all designs.

7.6 Convergence considerations

Convergence of the *APPS* optimisation algorithm to a local minimum was proved by *Kolda* [12], where the stopping criterion is based on the contraction of the search pattern size below a minimum relative step size in all search directions. If the step size used in producing the search patterns around the best current solution becomes too small to produce meaningful changes in the objective function, the algorithm can terminate after failing to expand the pattern size again due to the impact of numerical noise and modelling errors. As shown in Figure 13, where a minimum step size of 5% of the range of each variable was used, we obtained further improvements by restarting the optimisation from the best point obtained after the first search ended: restarting has the effect of maximizing the step size again.

As *APPS* focuses on the best current solution, lower ranking, but different and potentially

attractive designs can be found without getting explored further during the search. Using these solutions as seeds for additional optimisation runs afterwards can lead to interesting results and lower minimums.

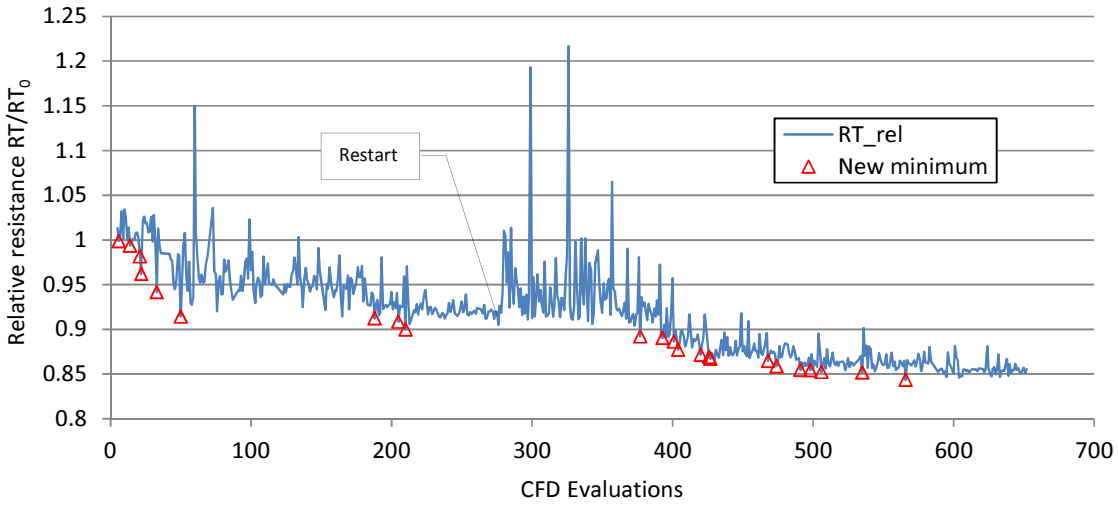

Figure 13 - Solution history for two cascaded *Parallel Pattern Search* runs.

8 CONCLUSIONS

We have created an interesting and original low-resistance hull shape of pre-determined length, displacement and stability using optimisation based on full viscous flow simulations. The approach we introduced to meet displacement and stability targets is particularly suited to the design of small to mid-size craft, where form stability dominates and the height of the centre of gravity doesn't normally represent a significant design challenge.

The work presented in this paper led to hulls offering approximately 50% less resistance throughout the displacement and transition speed ranges than the hard-chine lobster fishing vessel used as the source for representative initial stability and displacement figures.

9 ACKNOWLEDGMENTS

The authors want to thank *Friendship Systems AG* and *CD-Adapco*, which both made their software available for this work, as well as the *Australian Maritime College* at the *University of Tasmania* for providing access to their towing tank and supporting the experiments.

We also acknowledge the contribution of the *NeSI* high-performance computing facilities to the results of this research. New Zealand's national facilities are provided by the *New Zealand e-Science Infrastructure* and funded jointly by *NeSI*'s collaborator institutions and through the *Ministry of Business, Innovation & Employment*'s Research Infrastructure programme.

REFERENCES

[1] Oossanen, P.v., *Resistance prediction of small high-speed displacement vessels: State of the art.* International Shipbuilding Progress, 1980. **Vol. 27**(No. 313): p. 212-224.

[2] *CAESES / FRIENDSHIP-Framework*. Available from: https://www.caeses.com/.
[3] Biran, A. and R. López-Pulido, *Chapter 2 - Basic Ship Hydrostatics*, in *Ship Hydrostatics and Stability (Second Edition)*. 2014, Butterworth-Heinemann: Oxford. p. 23-75.
[4] Viola, I., R. Flay, and R. Ponzini, *CFD analysis of the hydrodynamic performance of two candidate America's Cup AC33 hulls.* International Journal of Small Craft Technology, Trans. RINA, 2012. **154**: p. B1.
[5] Brizzolara, S. and D. Villa. *CFD simulation of planing hulls*. in *Proceedings*. 2010.
[6] Böhm, C. and K. Graf, *Advancements in free surface RANSE simulations for sailing yacht applications.* Ocean Engineering, 2014. **90**: p. 11-20.
[7] *STAR-CCM+11.04.010-R8 User Manual.* 2016.
[8] Kelvin, L., *On ship waves.* Proc. Inst. Mech. Engrs, 1887. **38**: p. 409-434.
[9] Schlichting, H., *Boundary-Layer Theory*. 7th Ed ed. 1979, New York, U.S.A.: McGraw Hill.
[10] (ITTC), I.T.T.C., *Recommended Procedure 7.5-02-02-01, Resistance Test*, 2011.
[11] Haase, M., K. Zurcher, G. Davidson, J. Binns, G. Thomas and N. Bose, *Novel CFD-based full-scale resistance prediction for large medium-speed catamarans.* Ocean Engineering, 2016. **111**: p. 198-208.
[12] Kolda, T.G., *Revisiting Asynchronous Parallel Pattern Search for Nonlinear Optimization.* SIAM J. on Optimization, 2005. **16**(2): p. 563-586.
[13] *Dakota - Algorithms for design exploration and simulation credibility*. Available from: https://dakota.sandia.gov/.
[14] *HOPSPACK User Manual*. 2016; Available from: http://www.sandia.gov/hopspack/HopspackUserManual_2_0_2.pdf.